Fracture Mechanics of Concrete and Concrete Structures - High Performance, Fiber Reinforced Concrete, Special Loadings and Structural Applications- B. H. Oh, et al. (eds)

Unified model for mixed mode fracture of steel fibre reinforced concrete

T.N.S. Htut & S.J. Foster
School of Civil and Environmental Engineering, The University of New South Wales, Australia

ABSTRACT: For design with fibre reinforced concrete, engineers require a simple yet reliable approach that explains and models with sufficient accuracy material behaviour under load. In previous research, separate models have been developed to describe both Modes I and II fracture. This paper reviews the mechanical basis of these models and a unified model is developed using the variable engagement model (VEM) approach. The model is developed by integrating the behaviour of single, randomly oriented, fibres over 3D space and, based on quantifiable material and mix parameters, is shown to be capable of capturing the stress versus crack opening/sliding displacement response for steel-fibre reinforced composites in both the pre- and post-peak stages for Modes I and II fracture. In addition to describing both Modes I and II fracture in a rational way, it is hypothesised that the approach is valid for mixed mode fracture.

1 INTRODUCTION

Since Romualdi & Batson (1963) first performed tests on modern day fibre reinforced concrete (FRC), a significant body of research has been undertaken and reported in the literature. Studies such as those by Petersson (1980) have been undertaken on fibre reinforced concrete, with various percentages of fibres in the matrix, providing data on the tensile stress versus crack opening displacement (COD) response. Other studies, such as for example Banthia & Trottier (1994), have concentrated on the anchorage and pullout mechanisms of individual fibres crossing a joint in a tensile specimen while Lee & Foster (2006a) investigated fibres crossing a shear joint.

It is generally agreed that the mechanical properties such as ductility, durability, energy absorption, fatigue, increased service life and toughness of a quasi-brittle cement-based material can be significantly improved by reinforcing with fibres (Gopalaratnam & Shah, 1987, Guerrero & Naaman, 2000). In general the resistance to crack propagation depends on the bond resistance of the fibre that, in-turn, depends on the mechanical properties of the matrix and of the fibres such as geometry, orientation and length. There is no easy method to measure the bond stresses between fibres and a cementitious matrix, although fibre pullout tests have been used to determine average interfacial bond behaviour of fibre-matrix interfaces.

In a truly randomly orientated fibre reinforced concrete, few fibres are aligned in the direction of the applied load; instead, almost all fibres lie at an angle to the loading direction. In such cases, fibres are subjected to a combination of shear, bending and tensile stresses (Bartos & Duris, 1994). Due to their inclination angles, fibres bend at the exit point (i.e. at the crack interface) with snubbing of the fibres and spalling of the matrix expected for fibres at high inclination angles (Morton & Groves, 1974). In the Lee & Foster (2006b) and Htut & Foster (2008) study, radiographic imaging was used to highlight the importance of the snubbing effect in Modes I and II fracture.

Van de Loock (1987) considered combined shear and normal force in pre cracked push off specimens including hooked ended steel fibres with a diameter of 0.8 mm and length of 60 mm. The concrete compressive cube strength was 35 MPa. The different fibre volume concentrations considered in the tests were 0.0, 0.005 and 0.010 with a regression analysis then used to obtain a design equation. The restrictive nature of the Van de Loock equation, however, makes it unsuitable in the development of a general model.

Valle & Büyüköztürk (1993) investigated the behaviour of steel fibres as well as polypropylene fibres subjected to direct shear in both normal strength (29 MPa) and high strength (80 MPa) concrete. The effects from the addition and absence of stirrups across the shear plane were also studied. Crimped ended steel fibres with a length of 30 mm and diameter 0.5 mm were used in the tests with a fibre volume fraction of 0.01. Valle & Büyüköztürk used a shear transfer model to predict the stress strain behaviour of plain and fibre reinforced concrete. The method is comprehensive and involves a computational routine that requires solution of 11 non linear equations. Even though good agreement was ob-

tained between the experimental results and the proposed model, the Valle & Büyüköztürk technique cannot be readily applied and the results obtained are neither easily identifiable nor convenient in a shear stress-strain format.

Khaloo & Kim (1997) proposed an empirical shear transfer model to predict the shear stress and shear displacement behaviour of fibre reinforced concrete. The model is divided into two linear stages; first up to cracking and then to failure. Good agreement was obtained between the experimental results and the model. However, it was concluded by Lee & Foster (2006a, b) that the Khaloo & Kim tests are limited due to their mode of failure and the limited shear displacements measured. Mirsayah & Banthia (2002) performed shear tests on beam specimens in preference to the double L shaped specimens due to concerns that push off specimens did not accurately replicate pure shear once cracking had taken place. As for the model of Van de Loock, the regression modelling of Mirsayah & Banthia used to develop a design equation is limited by the range of test variables selected.

The application of existing models for general use is limited due to their restrictive or cumbersome nature and the regression approaches adopted by some researchers that, by definition, do not explain the mechanics. In this paper, a design model is developed that utilises data from individual fibre tests to develop a general modelling approach for mixed mode fracture of randomly orientated fibre reinforced concrete. The model is named the Unified Variable Engagement Model (UVEM).

2 UNIFIED VARIABLE ENGAGEMENT MODEL FOR MIXED MODE FRACTURE

2.1 *General*

It is well established for quasi-brittle materials loaded in tension and/or shear, such as concrete, that, after cracking, localization dominates the behaviour. Before cracking the behaviour can be expressed in terms of stress versus strain (Fig. 1), where H_0 is the elastic constant (for uniaxial tension, H_0 is the elastic modulus, for shear it is the shear modulus). After cracking, the localized behaviour is described by the load versus crack opening, or separation plane, w (Fig. 1).

In the model presented in this paper, it is postulated that the peak load for a discrete fibre embedded into a cementitious matrix can be used to determine the stress σ (over a plane of unit area) by summing the fibre (σ_f) and matrix (σ_c) contributions. That is

$$\sigma = \sigma_f + \sigma_c \tag{1}$$

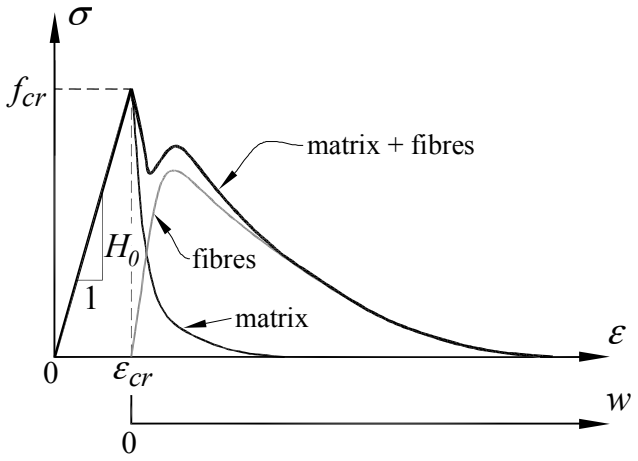

Figure 1. Stress versus strain/COD.

2.2 *Concrete component*

For an unreinforced concrete, the stress versus separation plane displacement can be taken as (Lee & Foster, 2007)

$$\sigma_c = c_1 \sigma_o e^{-c_2 w} \tag{2}$$

where σ_o is the strength of the concrete with $\rho_f = 0.0$ and c_1 and c_2 are coefficients. Defining ϕ as the angle between the direction of the applied load and a line normal to the separation plane (or crack) surface and γ as the angle between the direction of the applied load and an inclined discrete fibre (refer Fig. 2), then for $\phi = 0°$, σ_0 is equal to tensile strength of the concrete, while for $\phi = 90°$, σ_o is equal to the shear strength of the concrete (τ_0). The coefficient c_1 accounts for the beneficial effect of the fibres on the peak matrix strength.

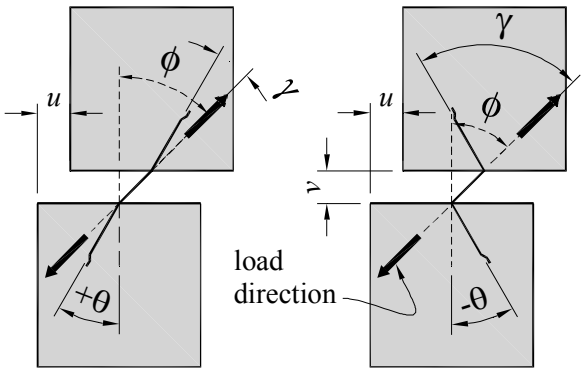

Figure 2. Discrete fibre orientation and definition of fibre bending angle, γ.

2.3 *Fibre component*

In the development of the UVEM, the following assumptions are made:

i the behaviour of a fibre reinforced composite may be obtained by a summation of its individual components; that is, the unreinforced matrix plus

each individual fibre can be added over the failure surface to give the overall response;

ii the geometric centres of the fibres are uniformly dispersed in space and all fibres have an equal probability of being oriented in any direction;

iii all fibres pullout from the side of the crack with the shorter embedded length while the longer side of the fibre is rigidly embedded in the matrix;

iv displacements due to elastic strains taking place within the fibres are small in comparison to the displacements arising from movement occurring between the fibres and the matrix; and

v the energy expended by bending of fibres compared to that of pullout of the fibres is small and can be neglected.

To define the relationship between a fibre and the direction of pullout relative to the matrix for mixed mode fracture, the fibre orientation angle, θ, is taken as measured from a line drawn normal to the separation plane (Fig. 2). A clockwise direction is taken as positive, whereas an anticlockwise direction is negative. The fibre bending angle, γ, and maximum fibre bending angle are then calculated as (Fig. 2)

$$\gamma = |\theta - \phi| \qquad (0 \leq \gamma \leq \pi) \tag{3}$$

$$\gamma_{max} = |\phi| + \pi/2 \qquad (\pi/2 \leq \gamma_{max} \leq \pi) \tag{4}$$

where the loading direction angle is $\phi = \tan^{-1}(u/v)$; $\phi = 0$ ($\gamma_{max} = \pi/2$) for Mode I and $|\phi| = \pi/2$ ($\gamma_{max} = \pi$) for Mode II fracture.

The crack displacement (w) is calculated from $w^2 = u^2 + v^2$, where u and v are the Mode II (sliding) and Mode I (opening) components, respectively. By definition, we take u and v always as positive.

Radiographic observations by Lee & Foster (2006b), Foster et al. (2007) and Htut & Foster (2007) show that it is possible to categorise the behaviour of a fibre crossing a crack using a few distinct zones (Fig. 3a) with each zone providing its own individual performance contribution (Fig. 3b). The component of shear in the straight section of a fibre between the hook and the snubbing region (σ_{st} in Fig. 3b) is small in comparison to that in the hooked zone (σ_{hook}) and the snubbing zone (σ_{snub}). The force carried by an individual fibre is then given as

$$P_f = P_{hook} + P_{snub} + P_{straight} \tag{5}$$

where P_{hook}, P_{snub} and $P_{straight}$ are the components carried by the hooked, snubbing and straight zones, respectively. A straight fibre may be treated as for a hooked fibre with the length of the hook taken as zero.

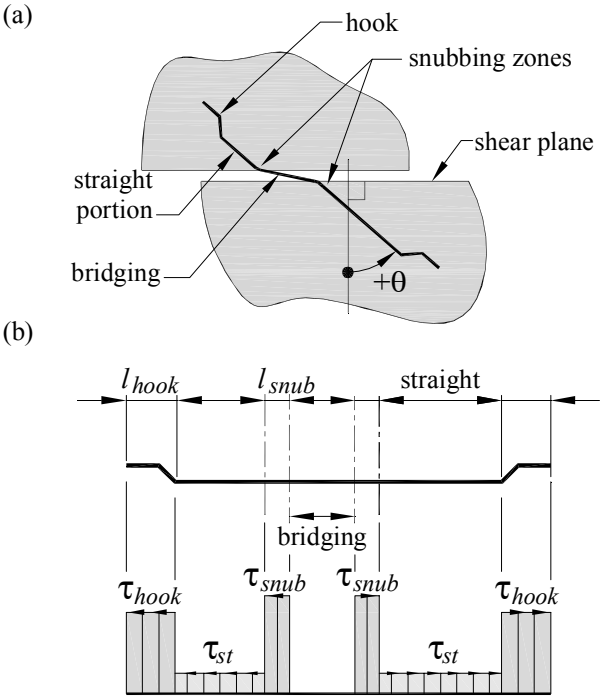

Figure 3. (a) Fibre performance zones and (b) shear contributions.

By way of example, for the Lee & Foster (2006a, b) and Htut & Foster (2007, 2008) test data on 60 mm long by 0.9 mm diameter, 1160 MPa, end-hooked (EH) fibres and 48 mm straight (S) fibres, with the S fibres produced by cutting off the hook of the EH fibres. The results are presented in Figure 4a with the specimens designated as X mm Y a:b, where X refers to fibre length, Y is the fibre type and a:b is the ratio of the fibre embedment length on the short side to that of the long side. It is observed from the figure that the contribution of the hooked end is, more or less, a constant with P_{hook} = 260 N. The contribution of the straight portion of the fibre is $P_{straight}$ = 80 N and the contribution of the snubbing increases with increasing γ. The contribution of each bond component (straight, snubbing and hook) is shown in Figure 4b. Also shown is the fibre fracture boundary; at large bending angles, fibres are increasingly prone to fracture as the snubbing bond increases. Such fibres provide only a short term benefit to the matrix upon their engagement and fibres at angles above the critical angle for fracture can be ignored in the development of the σ-w model.

In the development of the VEMI model (Voo, & Foster, 2004, 2009, Foster et al. 2006), a smeared bond model was used where the effects of bond were averaged over the fibre length. In the development of the VEMII model (Lee & Foster, 2007), both lumped and uniform bond models were developed. However, while the lumped model provides for a better physical description, the additional complexities in the model are not justified by a significantly higher level of accuracy. Thus, in the unified model

developed in this paper, the uniform bond modelling approach is adopted.

(a)

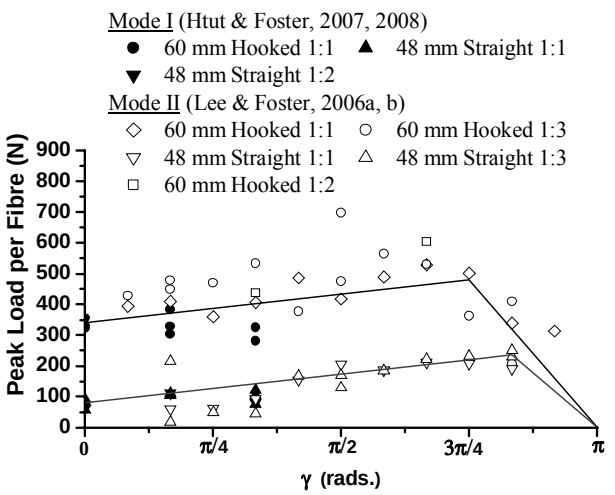

(b)

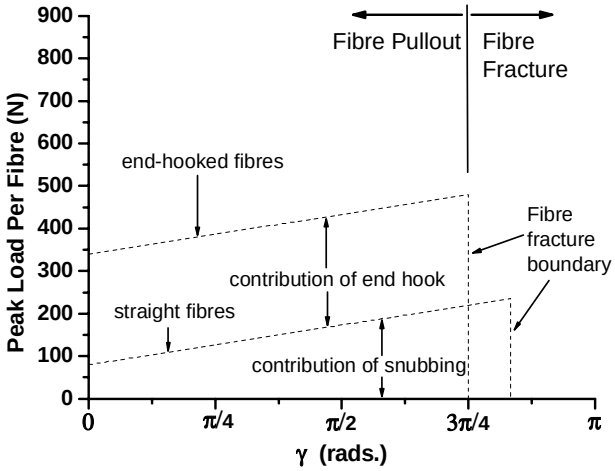

Figure 4. Peak load versus fibre bending angle, γ: (a) test data; (b) simplified design model.

With the uniform bond approach, the effects of each component (straight, snubbing and hook) are smeared along the remaining embedded length of the fibre. In Figure 5, the average bond stress obtained from the tests of Lee & Foster (2006a, b) and Htut & Foster (2007, 2008) are plotted against the fibre bending angle. Note that in this figure only the fibres with a 1:1 embedment ratio are considered. The smeared bond stress (τ_b) is calculated as

$$\tau_b = P_{f.max} / \left(\pi d_f l_a\right) \qquad (6)$$

where $P_{f.max}$ is the maximum force in the fibre and l_a is taken as the embedded length of the fibre at the point of engagement. In the model presented below, the point of engagement is taken as the crack (or separation plane) opening displacement corresponding to a force in the fibre of $0.5P_{f.max}$. Thus, in Equation 6 $l_a = l_f/2\text{-}w_e$, where w_e is the separation plane displacement at the point of engagement. The results show that the average bond stress along the fibre length may be expressed in the form

$$\tau_b = \tau_{b.0} + 0.25\gamma^3 \qquad (7)$$

where $\tau_{b.0}$ is the intercept bond stress (ie stress at $\gamma = 0$) and γ is in radians. For the 0.9 mm diameter fibres of this study, $\tau_{b.0}$ = 1.3 MPa for the S fibres and 4.1 MPa for the EH fibres. Note that Equation 7 is limited by the points corresponding to fibre fracture, which occurs at approximately $\gamma = 3/4\pi$ and $\gamma = 5/6\pi$ for the EH and S fibres, respectively (Fig. 4).

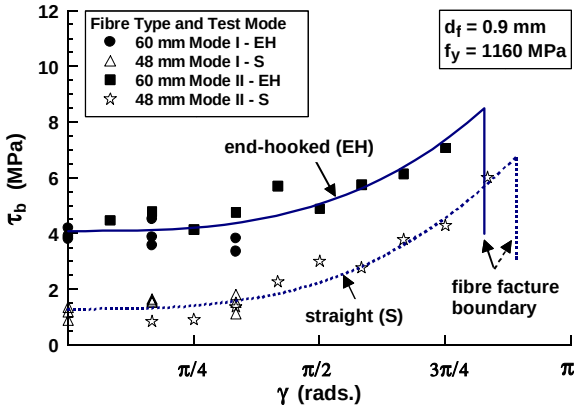

Figure 5. Bond stress at engagement versus fibre bending angle for 0.9 mm diameter fibres with Modes I and II test data.

In Figure 6, the model of Equation 7 is plotted for Mode I discrete fibre tests of Htut (2010) with the results for the intercept bond stress $\tau_{b.0}$, relative to the tensile strength of the mortar f_{ct}, summarised in Table 1. It is observed that the fibre diameter (d_f) and/or the strength of the fibre (σ_{fu}) are important parameters in determining bond resistance. It may be hypothesised that:

i the smaller the diameter of the fibre, the greater the propensity to cut through the matrix in the snubbing zone, thus increasing frictional the resistance; and

ii the higher the fibre strength, the more work that is required in the bending of the fibre as the hook pulls through the fibre tunnel.

There is insufficient test data to differentiate between these hypotheses and, thus, they remain open at this time.

Table 1. Bond stress to concrete tensile strength ratio.

Fibre Type	l_f (mm)	d_f (mm)	σ_{fu} (MPa)	$\tau_{b.0}/f_{ct}$ *
S	48	0.90	1160	0.5
EH	60	0.90	1160	1.6
S	23	0.55	1350	0.9
EH	35	0.55	1350	2.2
EH	25	0.30	2300	3.0

* f_{ct} = 2.5 MPa

A fibre will fracture when the tensile stress in the fibre exceeds its strength. A fibre will fracture at the hook if

$$P_{hook} > \sigma_{fu}\, \pi\, d_f^2 / 4 \qquad (8)$$

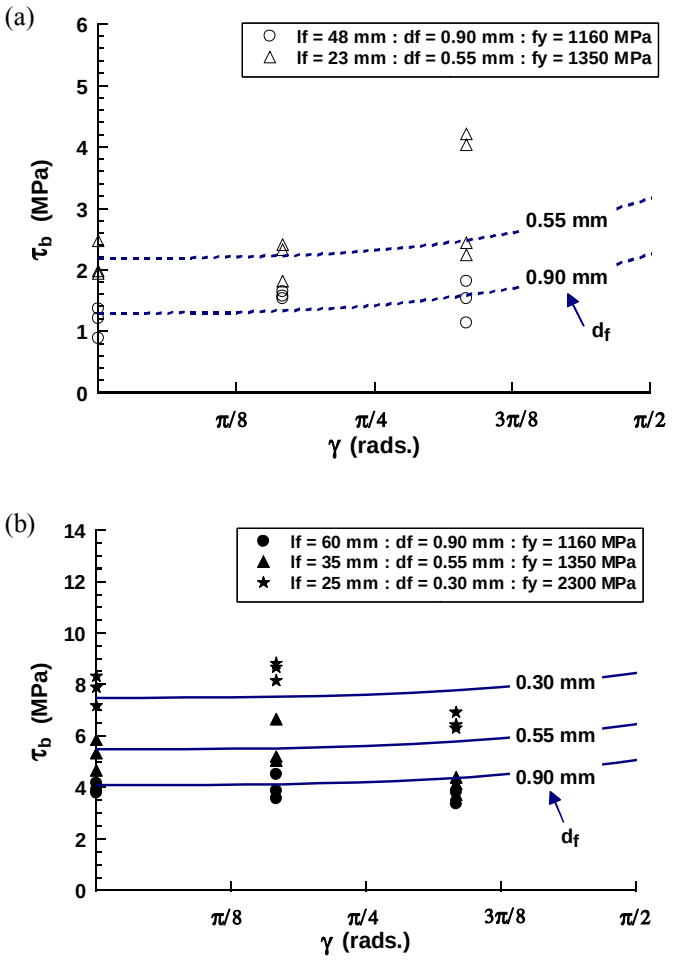

Figure 6. Bond stress at engagement versus fibre bending angle for Htut& Foster (2007, 2008) data: (a) S and (b) EH fibres.

where P_{hook} is the force in the hook and σ_{fu} is the strength of the fibre. For the 0.9 mm diameter fibres σ_{fu} = 1160 MPa; 260 N < $1160\pi 0.9^2/4$ = 740 N and, therefore, in this example, the hook will pullout from the matrix and not fracture. Similarly, a fibre will fracture in the snubbing region if the mechanical anchorage is such that the strength of the fibre is exceeded.

In the case of snubbing, a fibre is subjected to significant bending in addition to axial tension. For example, see the model of Voo & Foster (2004, 2009) for fibre fracture and bending. For the 0.9 mm diameter fibres, the straight fibres fracture at a load of approximately 240 N for a fibre bending angle of $\gamma = 5/6\pi$. Considering the effects of bending on the fibre strength, then the fibre will fracture if

$$P_{snub} > c\sigma_{fu}\pi d_f^2 / 4 \qquad (9)$$

$$c = \sigma_{fu}(\theta) / \sigma_{fu0} \qquad (10)$$

where $\sigma_{fu}(\theta)$ is the fracture strength for a fibre orientated at an angle θ to the separation (or cracking) plane and σ_{fu0} is the fibre strength when the bending stress is zero. For $\gamma = 5/6\pi$, we calculate from Equation 9 that $c = 0.32$. The issue of bending stresses, however, occurs only for fibres at large bending angles to the separation plane and its importance is diminished by other effects of snubbing such as the point of fibre engagement (ie that point where a fibre can be considered to be actively contributing to the strength of the composite). Taking the maximum embedded length of a fibre as $l_{a,max} = l_f/2$, the critical length of fibres such that fibre fracture need not be considered in the design model can be written as

$$l_f < l_c = \frac{d_f}{2} \times \frac{\bar{\sigma}_{fu}}{\tau_b} \qquad (11)$$

where $\bar{\sigma}_{fu}$ is an effective ultimate tensile strength of the fibre, considering fibre bending, and τ_b is the average bond stress along the fibre length.

Various models using the VEM approach for calculating the σ-w relationship are presented in Voo & Foster (2004, 2009) and Lee & Foster (2007). The models, however, are complex and before adding this additional level of complexity, the impact of fibre fracture and bending on the resulting σ-w curve needs first to be assessed.

Looking at the fibre fracture conditions, it is observed that fibre fracture is more likely for the higher bending angled fibres and these fibres do not engage until large separation displacements first occur. In the VEM approach, fibres at the large angles will pullout before engagement and do not contribute to the strength. Voo & Foster (2004, 2009) took the effective stress of the fibre for consideration of fibre fracture as $\bar{\sigma}_{fu} = \sigma_{fu}$, while for Mode II fracture Lee and Foster (2007, 2008) recommended $\bar{\sigma}_{fu} = 0.5\sigma_{fu}$. For the case of mixed mode fracture, it is suggested that fibre fracture need not be considered if Equation 11 is satisfied with

$$\bar{\sigma}_{fu} = \sigma_{fu} \times \pi/(2\gamma_{max}) \qquad (12)$$

If the inequality of Equation 11 is violated then a significant portion of the fibres may fracture and fibre fracture should be considered in calculating the σ-w curve. In the formulations that follow, it is taken that the effect of fibre fracture does not influence the outcomes of the model.

There are 4 possible states that an individual fibre can take in the UVEM model. They are:

1. the fibre is not engaged and may enhance the strength of the matrix when engagement is activated;
2. the fibre fractures upon engagement and, therefore, does not contribute to the strength of the

matrix;

3. the fibre is engaged and contributing to the strength of the matrix; and

4. the fibre was engaged but has since pulled out from the matrix and no longer adds to the strength of the matrix.

The significance of point 2 is that fibres at higher bending angles, γ, across the fracture surface do not need to be considered as the net (integrated) fibre contribution in that region is small as each fibre contributes to the strength of the matrix only over the small range of displacements from engagement to fracture (see Fig. 4b).

The force carried by a single fibre in a fibre composite is written the form

$$P_f = k\,\pi\, d_f\, \tau_b\, l_f / 2 \tag{13}$$

where k is the local orientation factor and is

$$k = 0 \qquad \text{for ..... } w < w_e \text{ and } w \geq l_a \tag{14a}$$

$$k = 2(l_a - w)/l_f \qquad \text{for ..... } w_e \leq w < l_a \tag{14b}$$

In Equation 14b, l_a is the initial fibre embedment length. For the case of discrete fibres in a cementitious matrix, the bond for the individual fibre τ_b is calculated from Equation 7 for a given fibre angle relative to the cracking and loading planes.

In VEMI (Voo & Foster, 2004, 2009, Foster et. al. 2006, Foster, 2009) and VEMII (Lee & Foster, 2007, 2008, Foster, 2009), the form of the engagement model adopted comes from the data on single fibre pullout tests. Taking the fibres as engaged at the point where the force in the fibre is $0.5P_{max}$, in the UVEM model of this study the fibre engagement function is proposed as

$$w_e = \alpha\, l_f \tan^3\left(\frac{\gamma}{\gamma_{max}} \cdot \frac{\pi}{2}\right) \tag{15}$$

By way of example, Equation 15 is plotted in Figure 7 for the individual fibre shear test data of Lee & Foster (2006a, b) and Htut & Foster (2008) for $\alpha = 1/(3.5\alpha_f)$, where $\alpha_f = l_f / d_f$ is the aspect ratio of the fibre. In these tests the fibres were 60 mm long by 0.9 mm diameter with end hooks.

Using the concept of a fibre engagement length, we can infer that for a randomly orientated fibre composite material subjected to any loading direction, at any point in the load versus separation plane displacement path there can be defined a critical angle for which fibres are becoming active. We term γ_{crit} as the point where fibres oriented at $\gamma \leq \gamma_{crit}$ carry load while for the fibres at $\gamma > \gamma_{crit}$, are yet to be engaged. Rearranging Equation 15 for the current opening displacement, w, leads to

$$\gamma_{crit} = \frac{2\gamma_{max}}{\pi} \tan^{-1} \sqrt[3]{\frac{w}{\alpha\, l_f}} \tag{16}$$

From Equation 17, fibres with $\gamma > \gamma_{lim}$ pullout from the matrix before engagement and, thus, these fibres are ineffective. Fibres at angles $\gamma \leq \gamma_{lim}$ may be engaged, depending on the initial embedment length, l_a.

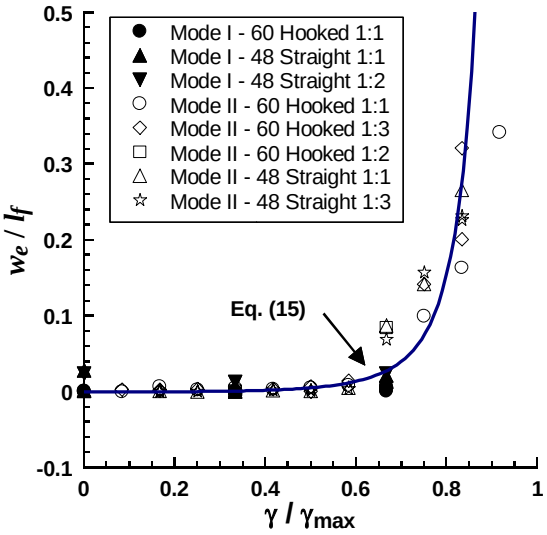

Figure 7. Fibre engagement ratio against fibre bending angle.

From Equation 16 it is clear that γ_{crit} is a function of the current separation plane displacement. Substituting the maximum possible fibre slip before engagement $w = l_f / 2$ into Equation 16 gives the limiting angles as

$$\gamma_{lim} = \frac{2\gamma_{max}}{\pi} \tan^{-1} \sqrt[3]{\frac{1}{2\,\alpha}} \tag{17}$$

Fibres orientated at angles $\gamma > \gamma_{lim}$ do contribute to the strength of the fibre composite at any point in the σ-w response.

To obtain the stress of the fibre composite at a given w, we integrate Equation 13 over a plane of unit area giving

$$\sigma_f = K_f \alpha_f \rho_f \tau_{b.ave} \tag{18}$$

where K_f is the global orientation factor and $\tau_{b.ave}$ is the average bond stress for all engaged fibres. The average bond stress is, in-turn, obtained from

$$\tau_{b.ave} = \frac{1}{\gamma_{crit}} \int_0^{\gamma_{crit}} \tau_b\, d\gamma \tag{19}$$

and substituting Equation 7 into Equation 19 gives

$$\tau_{b.ave} = \tau_{b.0} + 0.0625\,\gamma_{crit}^3 \tag{20}$$

The global orientation factor can be determined using probability theory and is affected by the shape of the domain over which the orientation is considered. The global orientation factor is calculated as

$$K_f = \frac{1}{N}\sum_{i=1}^{N} k_i \tag{21}$$

where N is the number of fibres crossing a plane of unit area and for the case of 3D randomly orientated fibres is given by $N = \rho_f/(2A_f)$, k_i is the local orientation factor for the i^{th} fibre, ρ_f is the volume fraction of fibres and A_f is the cross-sectional area of a single fibre.

Given a random distribution of fibres with equal probability that any given fibre crossing a crack has a shorter embedded length of between zero and $l_f/2$, the average value of the local orientation factor for all engaged fibres is

$$k_{ave} = \frac{1}{2} - \frac{w}{l_f} \tag{22}$$

If all fibre orientations have equal probability and noting that the proportion of bonded fibres decreases linearly with increasing w, then from Equation 16

$$K_f = \left(\frac{a+b}{\pi}\right)\left(1 - \frac{2w}{l_f}\right) k_{ave} \tag{23}$$

$$a = \min\left[\gamma_{crit}\,,\, \pi/2 - |\phi|\right] \tag{24}$$

$$b = \gamma_{crit} \tag{25}$$

where the term $(1–2w/l_f)$ is the proportion of fibres that have not pulled out from the matrix for a given crack opening-separation plane displacement. Finally, substituting Equation 22 into Equation 23 we find

$$K_f = \frac{1}{2}\left(\frac{a+b}{\pi}\right)\left(1 - \frac{2w}{l_f}\right)^2 \tag{26}$$

The stress versus crack opening-sliding response is then calculated from Equations 18, 20 and 26.

3 MODEL VERIFICATION

Ideally, to establish the fibre engagement curve (eg Fig. 7) individual fibre tests need to be undertaken on the specific fibre-matrix combination. In this paper, the Mode II fracture tests of Lee & Foster (2006a) with 35 mm long by 0.55 mm diameter EH fibres, and with fibre ratios of $\rho_f = 0.005$, 0.010, 0.015 and 0.020, are used to verify the performance of the model. For the fibre-concrete combination tested, the parameters of Equation 2 were measured as $c_1 = 1+72\rho_f$, $c_2 = 3.2$ and the shear strength for the case of $\rho_f = 0.0$ was measured as $\tau_o = 4.4$ MPa. The mean cylinder compressive strength of the mortar at the time of testing was $f_{cm} = 50$ MPa. From Table 1 for the 35 mm long by 0.55 mm diameter fibres, $\tau_{b.0} = 2.2 f_{ct}$ and taking $f_{ct} = \tau_o$ gives $\tau_{b.0} = 9.7$ MPa for this example.

The results of the model are compared against the test data in Figure 8 with a good correlation observed for displacements up to 10 mm. Beyond $w = 10$ mm, the assumption that a proportion of the fibres pullout from the longer embedded side becomes more important (refer Foster et al. 2007).

In a second example, the UVEM is compared with the Mode I fracture test results of Petersson (1980). In these tests, 30 mm long by 0.30 mm diameter straight steel fibres were used with fibre ratios of $\rho_f = 0.0025$, 0.010 and 0.015. The tensile strength of the mortar was measured to be $f_{ct} = 3.0$ MPa and considering the data of Table 1 for the 0.3 mm diameter fibres, the bond stress for $\gamma = 0$ is taken as $\tau_{b.0} = 1.2 f_{ct} = 3.6$ MPa. For the mortar component, Equation 2 was used with the tensile strength of concrete of $\sigma_o = 3$ MPa and with $c_1 = 1$ and $c_2 = 15$. The resulting stresses versus crack opening displacements are plotted in Figure 9. Again, a good agreement is seen for the model when compared with the experimental data.

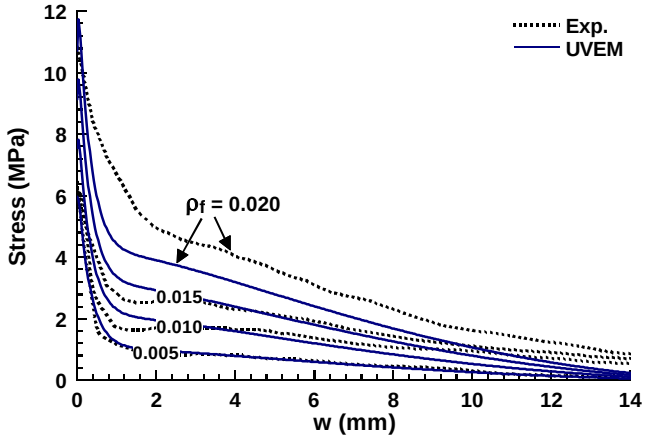

Figure 8. Comparison UVEM with Mode II test data of Lee & Foster (2006a) for 35 mm by 0.55 mm diameter EH fibres.

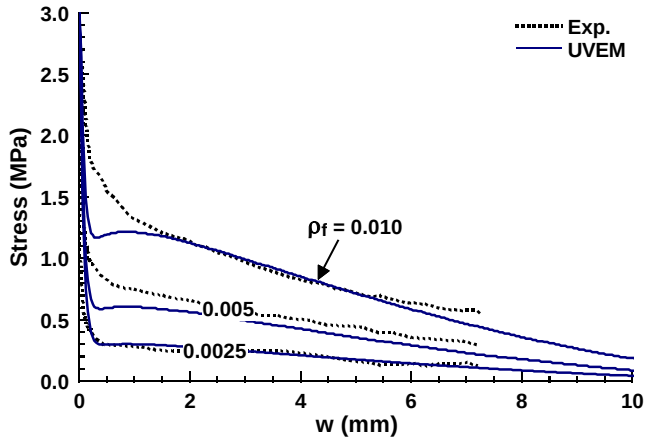

Figure 9. Comparison UVEM with Mode I test data of Petersson (1980) for 30 mm long by 0.3 mm diameter S fibres.

4 CONCLUSIONS

In this study a unified model has been developed to describe the stress versus crack opening displacement for a fibre reinforced concrete composite subjected to mixed mode fracture. The model is developed by integrating the effects of individual fibres crossing a cracking plane, together with the plain concrete component.

In the development of the unified model, the results and observations of discrete fibre tests were used, including visual data on the internal mechanisms obtained from x-ray and gamma ray imaging, to assess the contribution of each component of the fibre to the total. To this end, four distinct regions were identified as contributing to the overall behaviour; viz, the hook, the straight and snubbing portions and fibre bridging component. Of these regions, the hook (if any) and the snubbing zone were found to dominate the bond behaviour.

In the verification studies of UVEM, the model was compared against both Mode I and II experimental data and shows relatively good correlation with both modes of fracture. More data are needed, however, to test the model for mixed mode fracture.

5 ACKNOWLEDGEMENTS

This study was funded via Australian Research Council (ARC) discovery grant DP0559742. The support of the ARC is acknowledged with thanks.

REFERENCES

Banthia, N. & Trottier, J. F. 1994. Concrete reinforced with deformed steel fibres, Part I: Bond-slip mechanisms. *ACI Materials Journal*, 91 (5): 435-446.

Bartos, P.J.M. & Duris, M. 1994. Inclined tensile strength of steel fibres in a cement-based composite. *Composites*, 25 (10): 945-952.

Foster, S.J. 2009. The Application of Steel-Fibres as Concrete Reinforcement in Australia: from Material to Structure. *Materials and Structures*, 42(9): pp. 1209-1220.

Foster, S.J. et al. 2007. Radiographic imaging for the observation of Modes I and II fracture in fibre reinforced concrete. In Carpinteri, et al. (Eds.), *Fracture Mechanics of Concrete and Concrete Structures,* 6th International Conference on Fracture Mechanics of Concrete and Concrete Structures, Catania, Italy, Taylor & Francis, pp. 1457-1465.

Foster, S.J., et al. 2006. Analysis of Steel Fiber Reinforced Concrete Beams Failing in Shear: Variable Engagement Model", In Lowes, L., and Filippou, F (Eds), *Finite Element Analysis of Reinforced Concrete Structures*, Chapter 5, ACI SP-237.

Gopalaratnam, V.S. & Shah, S.P. 1987. Tensile failure of steel fibre-reinforced concrete. *Journal of Engineering Mechanics*, 113 (5): 635-652.

Guerrero, P. & Naaman, A.E. 2000. Effect of concrete fineness and adhesive agents on pullout response of steel fibres. *ACI Materials Journal*, 97 (1): 12-20.

Htut, T.N.S. 2010. Fracture Processes in Steel Fibre Reinforced Concrete. *PhD Thesis*, School of Civil and Environmental Engineering, The University of New South Wales, Australia (in prep.).

Htut, T.N.S. & Foster, S.J. 2007. X-Ray Imaging for the Observation of Mode I Fracture in Fibre Reinforced Concrete In Veidt, M. et al. (Eds.), *5th Australasian Congress on Applied Mechanics (ACAM),* Brisbane, Australia: pp. 120-125.

Htut, T.N.S. & Foster, S.J. 2008. Behaviour of steel fibre reinforced concrete and concrete in tension. In Aravinthan, T., Karunasena, W. & Wang, H. (Eds.), *Futures in Mechanics of Structures and Materials*, Toowoomba, Australia, Taylor & Francis, pp. 33-38.

Khaloo, A.R. & Kim, N. 1997. Influence of Concrete and Fiber Characteristics on Behaviour of Steel Fibre Reinforced Concrete under Direct Shear. *ACI Materials Journal*, 94 (6): 592-601.

Lee, G.G. & Foster, S.J. 2006a. Behaviour of steel fibre reinforced concrete in Shear I: Direct shear testing. *UNICIV Report R-444*, School of Civil & Environmental Engineering, The University of New South Wales, Sydney, Australia: 185 pp.

Lee, G.G. & Foster, S.J., 2006b. Behaviour of steel fibre reinforced concrete in Shear II: Gamma Ray imaging. *UNICIV Report R-445*, School of Civil & Environmental Engineering, The University of New South Wales, Sydney, Australia: 89 pp.

Lee, G. G. & Foster, S. J., 2007. Behaviour of Steel Fibre Reinforced Concrete in Shear III: Variable Engagement Model II. *UNICIV Report R-448*, School of Civil and Environmental Engineering, The University of New South Wales, Sydney, Australia: 106 pp.

Lee, G.G. & Foster, S.J. 2008. Modelling of shear-fracture of fibre-reinforced concrete. In Walraven, J. C. & Stoelhorst, D. (Eds.), *International FIB Symposium*, Amsterdam, CRC Press, pp. 493-499.

Mirsayah, A.A. & Banthia, N. 2002. Shear Strength of Steel Fibre-Reinforced Concrete. *ACI Materials Journal*, 99 (5): 473-479.

Morton, J. & Groves, G.W. 1974. The cracking of composites consisting of discontinuous ductile fibres in a brittle matrix-effect of fibre orientation. *Journal of Materials Science*, 9 (9): 1436-1445.

Petersson, P.E. 1980. Fracture mechanical calculations and tests for fibre-reinforced cementitious materials. *Proceeding, Advanced in Cement Matrix Composites*, Boston, Mat. Res. Soc., Annual Meeting, pp. 95-106.

Romualdi, J.P. & Batson, G.B. 1963. Behaviour of reinforced concrete beams with closely spaced reinforcement. *American Concrete Institute*, *Proceedings,* 60(6): 775-790.

Valle, M. & Büyüköztürk, O., 1993. Behaviour of Fiber Reinforced High Strength Concrete under Direct Shear. *ACI Materials Journal*, 90 (2): 122-133.
Van De Loock, L. 1987. Influence of Steel Fibres on the Shear Transfer in Cracks. *Proceedings of the International Symposium on Fibre Reinforced Concrete*, Madras, pp. 1.101-1.112.
Voo, J.Y.L. & Foster, S.J. 2004. Tensile-fracture of fibre-reinforced concrete: Variable engagement model In Di Prisco, M., Felicetti, R. & Plizzari, G. A. (Eds.), *Sixth RILEM Symposium on Fibre-Reinforced Concrete (FRC) - BEFIB*, Varenna, Italy, RILEM, pp. 875-884.
Voo Y.L. & Foster S.J. 2009. "Reactive Powder Concrete: Analysis and Design of RPC Girders", Lambert Academic Publishing, 364 pp.